Coordinate operation of power sources in a doubly-fed induction generator wind turbine/battery hybrid power system

Raúl Sarrias[a], Luis M. Fernández[b], Carlos A. García[b], Francisco Jurado[c,*]

[a] *Industrial Technologies Research Institute, University of Cádiz, 11202 EPS Algeciras, Algeciras (Cádiz), Spain*
[b] *Department of Electrical Engineering, University of Cádiz, 11202 EPS Algeciras, Algeciras (Cádiz), Spain*
[c] *Department of Electrical Engineering, University of Jaén, 23700 EPS Linares, Linares (Jaén), Spain*

ARTICLE INFO

ABSTRACT

This paper deals with the modeling and control of a hybrid system integrating a doubly-fed induction generator (DFIG) wind turbine and batteries as energy storage system (ESS). The modeling of the mechanical and electrical main components of a 1.5 MW wind turbine is described. Specific focus is to be taken on the power converter of the DFIG, since it allows the interconnection of the ESS to the generator and a proper energy management. A lead-acid battery is used as energy storage device, which is connected through a bidirectional DC/DC converter to the DC bus of the DFIG power converter. A new supervisory control system, responsible for the coordinate operation of power sources (DFIG wind turbine and ESS), is described and evaluated by simulation under wind speed fluctuations and grid demand changes. It is based on using the wind turbine as primary power source and the ESS as auxiliary power source, providing or storing the power mismatching between the actual wind power and grid demand, whenever the battery state-of-charge (SOC) remains within the recommended limits. This configuration increases the generation capability and smooths the output power fluctuations caused by the wind speed variability, and therefore, improves the grid integration of wind turbines.

1. Introduction

In the recent years, wind power generation is experiencing a remarkable growth in terms of installed power and energy generation in many countries. USA and China are currently the world leaders in installed wind power [1]. In Europe, Germany and Spain lead the total cumulative installed capacity. The expansion of this renewable resource has also led to important improvements in the technology of wind turbines and auxiliary equipment. Nonetheless, wind power generation presents certain characteristics that hamper a broader penetration, especially in weak grids [2–4]. Since wind energy is based upon a natural resource, it is an intermittent, uncontrollable, and, to some extent, unpredictable energy source. Therefore, many authors have dealt with the uncertainty that a high penetration of wind power in electric power systems involves [2–7].

Energy storage systems (ESS) are regarded as a viable solution to some of these problems [2–5,8–11]. In [10,12–15], different aspects of several energy storage technologies are studied for wind power and other renewable energy applications. Some devices, such as batteries, flywheels, superconducting magnetic energy storage (SMES), supercapacitors, compressed air energy storage (CAES), hydropumped storage or hydrogen technology, are considered appropriate for reducing the power output fluctuations in wind farms. Among them, batteries are known to provide an adequate behavior with high power or energy requirements [16,17]. Furthermore, lead-acid batteries are the oldest and most mature technology [14–17], and have shown acceptable performance in large scale applications [16]. For these reasons, they have been chosen in this work to operate coordinately with the wind turbine.

For variable speed wind turbines, DFIG and permanent magnet synchronous generator (PMSG) are the most outstanding technologies [18–21]. Their modeling and simulation together with different ESS has been addressed in [4,21–24]. However, in some of these cases [4,21,22], the ESS is placed somewhere between the wind turbine output and the grid, which contrasts with the ESS location and energy management philosophy proposed herein. Currently, the most widely used wind turbine is based on a DFIG, since it operates at variable speed by the use of a partial power converter of 25%–30% of the generator-rated power, which makes it advantageous from an economic point of view. Furthermore, this system allows reactive power compensation and smooth grid connection [18–20]. For these reasons, a DFIG has been considered in this work. Its structure allows connecting the ESS to the DC bus, within the generator

circuitry itself, and therefore, before the point of common coupling to grid. Furthermore, the active and reactive power generation can be controlled by acting on the power converter of the DFIG [23,24].

In this work, a hybrid wind turbine integrating an ESS is modeled using MATLAB-Simulink® of MATLAB. A DFIG wind turbine of 1.5 MW rated power is considered. The control implemented for the proper operation of the DFIG wind turbine is described. As ESS, a lead-acid battery has been modeled. It is coupled to the DC bus of the DFIG wind turbine through a bidirectional DC/DC converter. This battery will either provide or store energy depending on the available wind power and grid demand. The coordinate operation of DFIG and ESS is managed by a supervisory control system. It defines the power reference for the ESS depending on its state-of-charge (SOC), actual wind power generation and grid demand. The model and control of hybrid wind turbine have been evaluated by simulations under wind speed fluctuations and grid power demand changes.

This paper is organized as follows: Section 2 presents a general description of the hybrid system. The modeling of the mechanical and electrical main components of the wind turbine is dealt in Section 3. Section 4 describes the modeling of the ESS and its connection to the DFIG power converter. The control systems developed for the wind turbine and ESS power converters are illustrated in Section 5. The supervisory control system is explained in Section 6. The simulation results are presented and discussed in Section 7. Finally, conclusions are drawn in Section 8.

2. DFIG wind turbine with ESS

Fig. 1 shows the configuration adopted for the DFIG wind turbine with battery as ESS.

A DFIG wind turbine presents a wound rotor induction generator coupled to the wind turbine through a gearbox. The wind turbine uses blade pitch angle control in order to limit the power and the rotational speed for high winds. DFIG presents the stator winding connected directly to the grid and a bidirectional power converter feeding the rotor winding. It is made up of two back-to-back IGBT bridges linked by a DC bus. The rotor side converter (RSC), connected to the rotor winding, converts the low AC frequency of the generator to DC. The DC voltage is stabilized by DC link capacitor, and converted further by the grid side converter (GSC) into AC, which is supplied to the grid.

A rechargeable lead-acid battery is used as electrical energy storage. This battery is connected to the DC bus through a bidirectional DC/DC converter, which allows the charge and discharge of the battery. Through the DC link, the active power consumed/generated by the DFIG rotor winding and by the battery is provided to the GSC, and from this converter, it is fed to the grid. The DC link contains a capacitor that is charged/discharged by the RSC, GSC and battery currents, respectively.
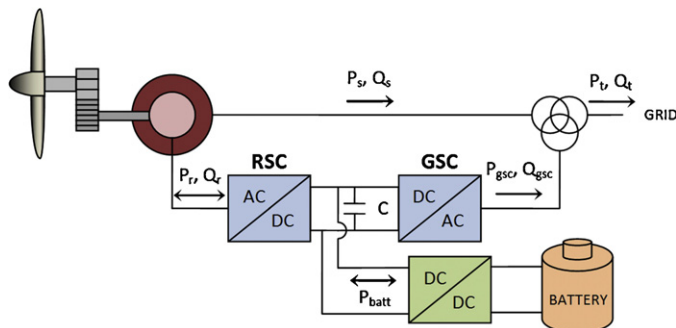

Fig. 1. DFIG wind turbine with ESS based on battery.

3. Modeling of the DFIG wind turbine

In this work, it was modeled a General Electric (GE) 1.5 MW DFIG wind turbine [25]. The used model is based on the model included in SimPowerSystems® [26], which has been modified in order to allow a proper control of the hybrid system (DFIG including the ESS). This model is composed of the following subsystems: (1) mechanical system; and (2) electrical system. The modeling of these subsystems is described next.

3.1. Mechanical system model

The mechanical system of the DFIG wind turbine consists of: (A) aerodynamic rotor and (B) drive train.

3.1.1. Aerodynamic rotor

The rotor of the wind turbine is the first element facing the incoming wind. It consists of the blades and the hub, coupled to the drive train in the nacelle. Therefore, the rotor captures the wind power and provides a mechanical torque to the drive train. Its behavior was modeled using the actuator disk theory [27], according to which, the mechanical power absorbed by the wind turbine (P_{wt}) is given by:

$$P_{wt} = \frac{1}{2} \cdot \rho \cdot A \cdot C_p(\lambda, \theta) \cdot u^3 \tag{1}$$

where ρ is the wind density, A is the area of the rotor disk, u is the incoming wind speed, and C_p is the power coefficient. The power coefficient expresses the rotor aerodynamics as a function of both tip speed ratio λ and the pitch angle of the rotor blades θ. The C_p curves of the wind turbine modeled in this work are shown in Fig. 2.

The mechanical torque developed by the wind turbine, T_{wt}, can be obtained dividing the mechanical power P_{wt} by the rotating speed of the wind turbine ω_{wt}.

$$T_{wt} = \frac{P_{wt}}{\omega_{wt}} \tag{2}$$

This torque is transmitted from the drive train to the electric generator through a gear box that increases the rotational speed to that required by the DFIG rotor.

3.1.2. Drive train

The drive train connects the DFIG rotor with the aerodynamic rotor, and therefore, it transmits the mechanical power to the electrical generator through the rotating shafts and the gearbox. The modeling of the drive train is commonly carried out using the well-known two-mass dynamic model [27]. This model is composed of two masses, aerodynamic rotor and generator rotor, elastically connected via springs. This coupling is characterized by its stiffness and damping factor. The model is expressed by the following equations:

$$T_{wt} - T_{mec} = J_{wt} \cdot \frac{d\omega_{wt}}{dt} \tag{3}$$

$$T_{mec} = D_{dt} \cdot (\omega_{wt} - \omega_r) + K_{dt} \cdot \int (\omega_{wt} - \omega_r)dt \tag{4}$$

$$T_e - T_{mec} - \omega_r \cdot F = J_r \cdot \frac{d\omega_r}{dt} \tag{5}$$

where T_{wt} represents the mechanical torque from the aerodynamic rotor shaft, T_{mec} is the mechanical torque from the generator shaft, T_e is the generator electrical torque, J_r is the aerodynamic rotor inertia, J_g is the generator inertia, K_{dt} and D_{dt} are the stiffness and damping of mechanical coupling, ω_r is the generator angular velocity and F is the viscous friction coefficient from the generator shaft.
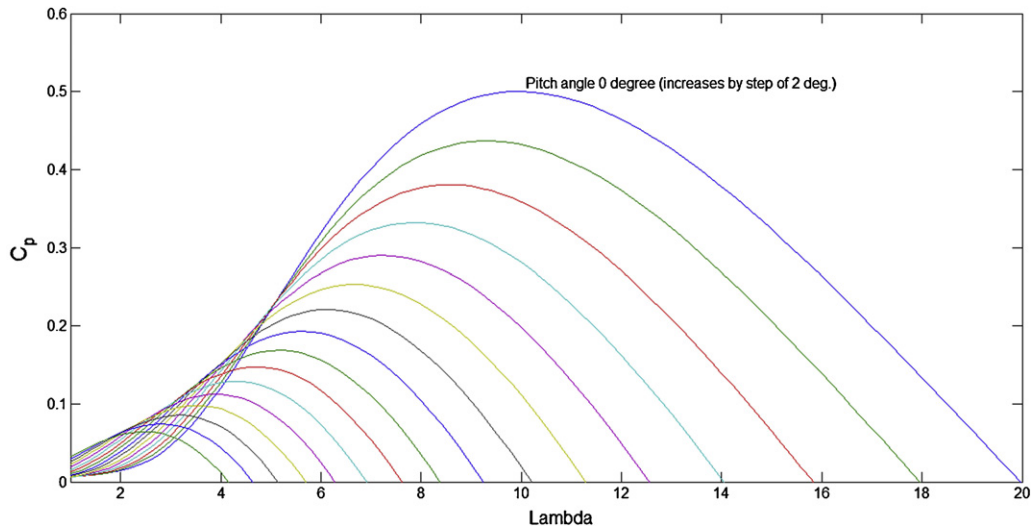
Fig. 2. C_p curves of the wind turbine.

3.2. Electrical system model

The electrical model of the wind turbine is basically composed of the DFIG and the power converter.

3.2.1. DFIG

A fifth-order model of the DFIG was implemented [28]. This model is composed of four electrical differential equations (two equations for both the stator and rotor voltages) and one mechanical differential equation (included in the drive train model). The electrical equations, expressed in direct (d)–quadrature (q) coordinate reference frame rotating at synchronous speed ω_s, are given by:

$$u_{ds} = R_s \cdot i_{ds} + \frac{d}{dt}\varphi_{ds} - \omega \cdot \varphi_{qs}$$
$$u_{qs} = R_s \cdot i_{qs} + \frac{d}{dt}\varphi_{qs} + \omega \cdot \varphi_{ds} \tag{6}$$

$$u_{dr} = R_r \cdot i_{dr} + \frac{d}{dt}\varphi_{dr} - (\omega - \omega_r) \cdot \varphi_{qr}$$
$$u_{qr} = R_r \cdot i_{qr} + \frac{d}{dt}\varphi_{qr} + (\omega - \omega_r) \cdot \varphi_{dr} \tag{7}$$

where u denotes voltage, i denotes current, φ represents magnetic flux, R denotes resistance and L inductance, indexes d and q stand for the direct and quadrature components, and indexes s and r refer to stator and rotor respectively.

The flux linkages are expressed as follows:

$$\varphi_{ds} = L_s \cdot i_{ds} + L_m \cdot i_{dr}$$
$$\varphi_{qs} = L_s \cdot i_{qs} + L_m \cdot i_{qr} \tag{8}$$

$$\varphi_{dr} = L_r \cdot i_{dr} + L_m \cdot i_{ds}$$
$$\varphi_{qr} = L_r \cdot i_{qr} + L_m \cdot i_{qs} \tag{9}$$

where index m denotes magnetizing.

The generator electromechanical torque is calculated as follows:

$$T_e = 1.5 \cdot p \cdot (\varphi_{ds} \cdot i_{qs} - \varphi_{qs} \cdot i_{ds}) \tag{10}$$

where p is the number of pair poles.

3.2.2. DFIG power converter

The power converter that electrically connects the rotor windings of the generator with the grid allows variable speed operation of the DFIG. As previously mentioned, it presents a two back-to-back IGBT bridges (RSC and GSC) linked by a DC bus, which presents a stabilizing capacitor. On the whole, the converter is modeled as an AC/DC/AC PWM converter based on IGBT switches.

The RSC regulates the rotor voltage in order to achieve the power reference defined by the control system. This converter drives the wind turbine to achieve the optimum power efficiency in winds below rated, to limit the output power to the rated value in winds above rated, or to adjust both the active and reactive powers to the power references when power regulation is demanded [19].

On the other hand, the GSC acts on the grid side voltage in order to maintain the exchange active power from the rotor circuit and/or the battery to the grid, and to operate with a defined power factor, commonly unity power factor (zero reactive power) [19].

Through the DC link, the active power generated by the DFIG through the RSC and provided by the battery is supplied to the GSC, and from this converter, it is fed to the grid. The DC bus contains a capacitor that is charged/discharged by RSC, GSC and battery currents, respectively. When the power is dynamically changed between the GSC and RSC, the instantaneous power of the DC bus capacitor changes, which makes the DC bus voltage fluctuate. These DC voltage fluctuations can be stabilized by a proper control of the battery converter. The control implemented in the converters is described in detail in Section 5.

4. Modeling of the energy storage system

The ESS considered in this work is composed of a lead-acid battery, which is connected to the DC bus of the DFIG through a bidirectional DC/DC power converter. The modeling of these components is described next.

4.1. Battery

In this work, it was developed a model of the lead-acid electrochemical battery, whose characteristic parameters were selected from a commercial battery, Discover's D21000, which is specially designed for renewable energy applications [29]. The battery was sized in terms of minimum capacity, so that its maximum instantaneous power is limited by the power of GSC. Connecting cells in series and parallel, a 585 Ah, 624 V battery was accomplished.

The lead-acid battery was modeled by the battery model included in SimPowerSystems [26], where it is modeled as a
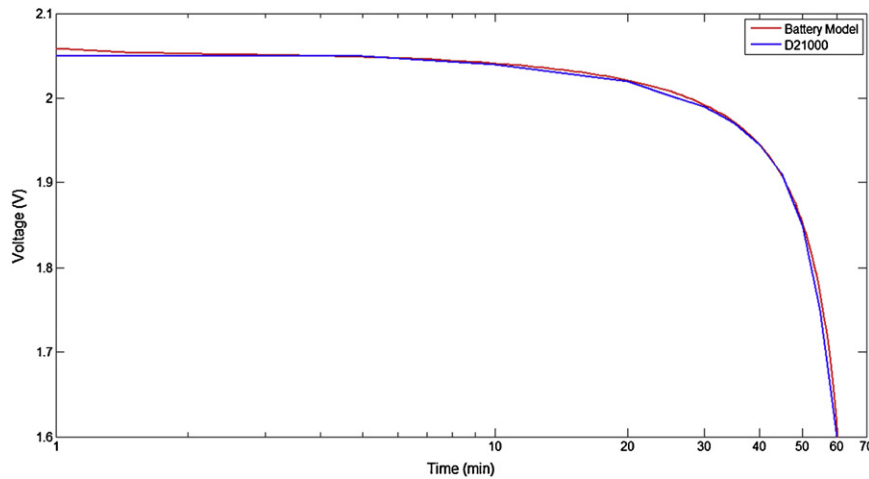
Fig. 3. Discharge curves for the commercial and modeled battery.

variable voltage source in series with an equivalent internal resistance. The battery voltage is given by:

$$U_{bat} = E_{bat} - R_i \cdot i \tag{11}$$

where U_{bat} is the battery voltage, E_{bat} is the no load voltage, i is the battery current, and R_i is the battery internal resistance, which is assumed to be constant during the charge and the discharge cycles, and which does not vary with the amplitude of the current.

The no load voltage during the charging or discharging of the battery depends on the battery current, extracted capacity, and hysteresis phenomenon of the battery during the charge and discharge cycles. It can be calculated as follows:

$$E_{bat\,disch} = E_0 - K \cdot \frac{Q}{Q - i_t} \cdot i^* - K \cdot \frac{Q}{Q - i_t} \cdot i_t + f_{hyst\_disch}(i) \tag{12}$$

$$E_{bat\,char} = E_0 - K \cdot \frac{Q}{|i_t| + 0.1 \cdot Q} \cdot i^* - K \cdot \frac{Q}{Q - i_t} \cdot i_t + f_{hyst\_char}(i) \tag{13}$$

where E_0 is the constant voltage, K is the polarization constant or polarization resistance, i^* is the low-frequency current dynamics, i is the battery current, i_t is the extracted capacity; Q is the maximum battery capacity, and $f_{hyst\_char}(i)$ and $f_{hyst\_disc}(i)$ are functions of the battery current, which represent the hysteresis phenomenon of the battery during the charge and discharge cycles.

In most electrochemical batteries, it is important to maintain the SOC within certain recommended limits in order to avoid internal damage of the device. Therefore, a proper control of the battery SOC was applied in this work in order to maintain it between 30 and 70%. The instantaneous value of the SOC is calculated as follows:

$$SOC(\%) = 100 \cdot \left(1 - \frac{\int i\,dt}{Q}\right) \tag{14}$$

Fig. 3 shows the discharge curve of the battery provided by the manufacturer and that obtained with the model implemented in this work. As can be seen, the agreement is quite acceptable.

4.2. Battery power converter

The electrochemical battery is connected to the DC bus of the DFIG through a bidirectional DC/DC power converter. Hence, the current and power flows from/to the battery when the power is dynamically changed between the GSC and RSC, thus allowing both discharge and charge cycles of the battery. Furthermore, this converter helps maintaining the DC bus rated voltage while the battery voltage varies depending on the operating conditions.
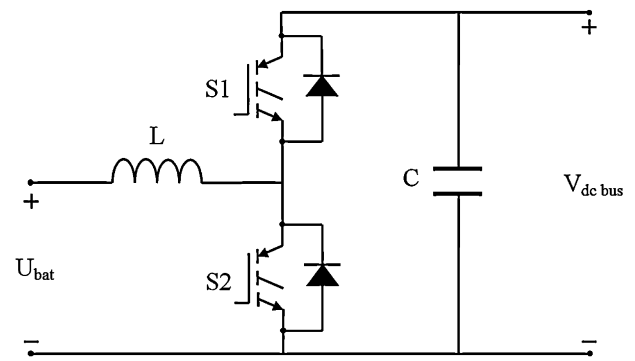

Fig. 4. Bidirectional DC/DC battery power converter.

Fig. 4 presents the configuration of the bidirectional DC/DC power converter used in this work. It consists of a high-frequency inductor, an output filtering capacitor, and two IGBT-diodes switches. When the battery charges, the energy flows from the DC bus to the battery through the S_1 switch and S_2 diode. Therefore, the converter acts as a unidirectional buck converter. On the other hand, the battery discharges through the S_2 switch and S_1 diode, providing energy to the DC bus. In this case, the converter acts as a unidirectional boost converter.

The battery power converter was modeled using the two-quadrant chopper model included in SimPowerSystems. It is controlled for DC bus voltage regulation [30,31]. In fact, effective control of the duty cycle of the bidirectional converter enables a suitable control of the DC bus voltage and the charge and discharge of the battery. The control scheme implemented is discussed later on.

5. Control systems of the wind turbine and ESS

In this section, the control systems applied to the wind turbine and battery are described. Four controllers were implemented in the model: (A) pitch angle control, (B) RSC control, (C) GSC control, and (D) battery power converter control. They allow the wind turbine and battery to achieve the operation required by the supervisory control system of the hybrid system.

5.1. Pitch angle control

The pitch angle controller adjusts the blade pitch angle reducing the power coefficient and thus the power extracted from the
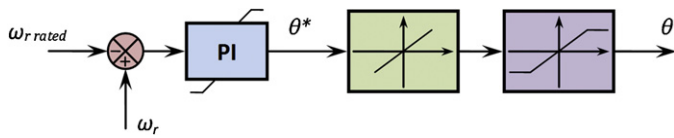
Fig. 5. Pitch angle control scheme.

wind when the rotational speed increases up to the rated speed. The controller keeps the optimal pitch angle when the generator speed is less than the rated speed, and thus the wind turbine operates with optimum power efficiency. On the other hand, when the wind turbine operates with power limitation or power reduction, this controller limits the rotational speed to the rated speed. Therefore, the blade pitch angle controller acts as a rotational speed limiter in any operating conditions [19].

Fig. 5 shows the control scheme implemented, which includes the rate and angle limiters of the pitch angle movement that the real actuator presents.

5.2. RSC control

The control strategy implemented in the RSC allows the decoupled control of the active and reactive powers by acting on the d and q components of the rotor voltage, respectively. The control scheme applied to the RSC is shown in Fig. 6.

Because the d-axis of the reference frame is oriented along the stator voltage vector, then the component u_{qs} is zero. When Eqs. (6)–(9) are combined and the stator resistance is neglected, it is obtained the following expressions for the components of rotor voltage:

$$u_{dr} = R_r \cdot i_{dr} - (\omega - \omega_r) \cdot L_r \cdot i_{qr} - (\omega - \omega_r) \cdot L_m \cdot i_{qs} + u'_{dr} \quad (15)$$

$$u_{qr} = R_r \cdot i_{qr} + (\omega - \omega_r) \cdot L_r \cdot i_{dr} + (\omega - \omega_r) \cdot L_m \cdot i_{ds} + u'_{qr} \quad (16)$$

where u'_{dr} and u'_{qr} can be expressed as a function of i_{dr} and i_{qr} respectively.

The total active power generated by the DFIG (P_g) is calculated from the sum of the stator power (P_s) and the power flowing through the rotor windings (P_r). Hence, these three powers are expressed as follows:

$$P_s = 1.5 \cdot (u_{ds} \cdot i_{ds} + u_{qs} \cdot i_{qs}) \quad (17)$$

$$P_r = 1.5 \cdot (u_{dr} \cdot i_{dr} + u_{qr} \cdot i_{qr}) \quad (18)$$

$$P_g = P_s + P_r \quad (19)$$

When Eqs. (6)–(9) and (17) and (18) are combined and the stator resistance is neglected, it is obtained that the total active power can be expressed as directly dependent on the d component of the rotor current and subsequently, on the d component of the rotor voltage, as deduced from Eq. (15).

As shown in Fig. 6, the u_{dr} controller is an active power controller that controls the output power by acting on the d component of the rotor voltage. This controller presents a selector to choose the operating mode. Two operating modes can be selected: power optimization/limitation and power reduction.

In the power optimization/limitation mode, the RSC controller uses the power–speed curve to define the active power reference according to the actual rotational speed. As a consequence, the wind turbine can operate with variable speed maximizing the power extracted from the wind in winds below rated or limiting the output power to rated power in winds above rated. In the power reduction mode, the controller uses the value ordered by the supervisory control system as a power reference, instead of the power reference derived from the power–speed curve.

Similarly to the active power, the reactive power that a DFIG wind turbine exchanges with the grid (Q_t) is the sum of that delivered by the stator windings (Q_s) and the amount transferred through the GSC (Q_{gsc}). However, it is equal to the stator reactive power, since the GSC usually operates with unity power factor.

$$Q_t = Q_s = 1.5 \cdot (u_{qs} \cdot i_{ds} - u_{ds} \cdot i_{qs}) \quad (20)$$

When Eqs. (6)–(9) and (20) are combined and the stator resistance is neglected, it is obtained that the total reactive power can be expressed as directly dependent on the q component of rotor current. Subsequently, the reactive power can be expressed as directly dependent on the q component of the rotor voltage u_{qr}, as deduced from Eq. (16).

The u_{qr} controller, shown in Fig. 6, determines the quadrature component of rotor voltage, enabling the wind turbine operation with the desired reactive power.

Once the rotor voltage references (u_{dr} and u_{qr}) are generated, a PWM generator provides a six-component vector containing the duty cycles of the IGBT switches included in the RSC. Finally, the magnitude of the three-phase rotor voltage injected to the rotor windings u_{rabc} is obtained.
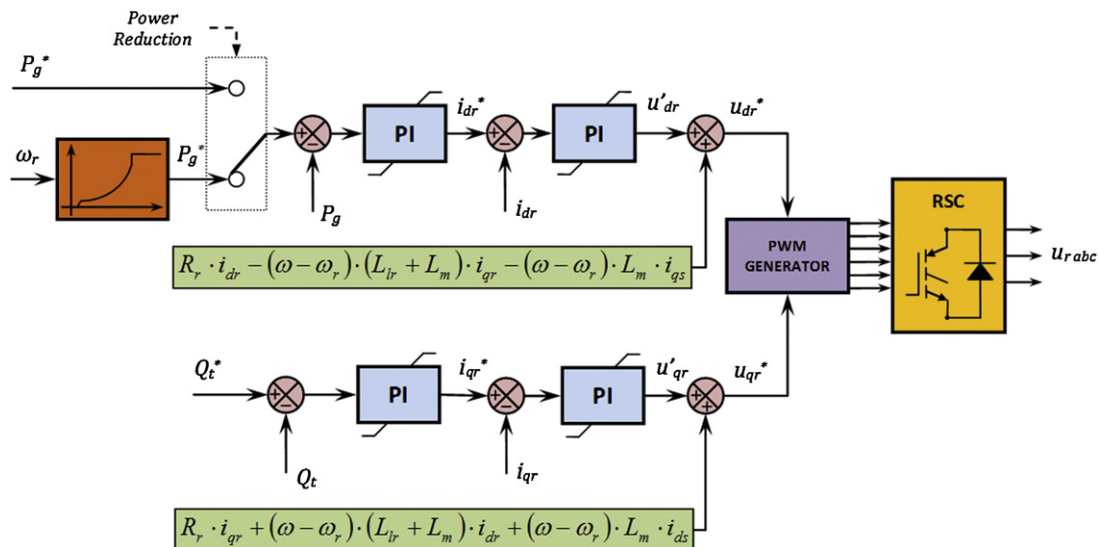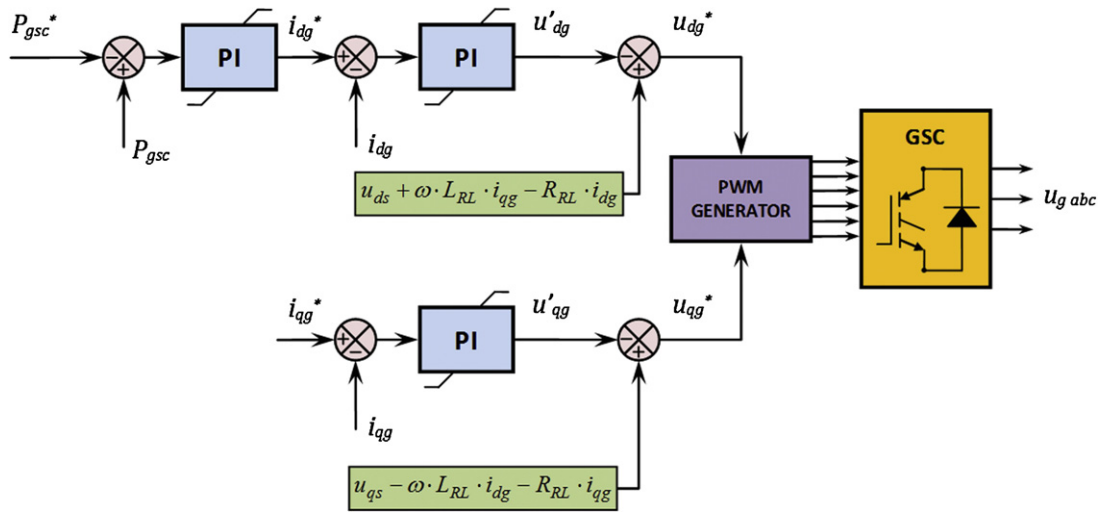

Fig. 6. RSC control scheme.

Fig. 7. GSC control scheme.

5.3. Grid side converter control

A similar control strategy was applied to the GSC, since the active and reactive powers of the GSC can be controlled independently by acting on the d and q components of the grid side voltage. This voltage can be expressed as follows:

$$u_{dg} = u_{ds} - R_{RL} \cdot i_{dg} + \omega \cdot L_{RL} \cdot i_{qg} - u'_{dg} \qquad (21)$$

$$u_{qg} = u_{qs} - R_{RL} \cdot i_{qg} - \omega \cdot L_{RL} \cdot i_{dg} - u'_{qg} \qquad (22)$$

where u_{dqg} represents the AC voltage at the grid side of the converter, R_{RL} and L_{RL} are the components of the impedance of the filter between the GSC and the grid, and i_{dqg} is the current flowing through the converter.

The voltages u'_{dg} and u'_{qg} can be expressed as a function of i_{dg} and i_{qg} respectively. Subsequently, the u_{dqg} reference is generated by a PI controller-based control loop, according to the control scheme shown in Fig. 7. The PI controllers are used to regulate the active and reactive powers transferred to grid.

The active power that the GSC delivers to grid can be expressed by:

$$P_{gsc} = 1.5 \cdot (u_{dg} \cdot i_{dg} + u_{qg} \cdot i_{qg}) \qquad (23)$$

Because the d-axis of the reference frame is oriented along the grid voltage, the component u_{qg} is zero. Then, the GSC active power can be expressed as directly dependent on the i_{dg}, and therefore on u_{dg}, as deduced from Eq. (21). The outer loop of u_{dg} controls the GSC in order to adjust the active power P_{gsc} to the power reference P_{gsc}^*. This power reference is determined from the difference between the active power flowing through the RSC, and the power to be stored in or provided by the battery, which is defined by the supervisory control system.

The reactive power transferred from/to the grid through the GSC can be expressed as:

$$Q_{gsc} = 1.5 \cdot (u_{qg} \cdot i_{dg} - u_{dg} \cdot i_{qg}) \qquad (24)$$

The reactive power Q_{gsc} depends directly on i_{qg}, since the component u_{qg} is zero. GSC usually operates with unity power factor, and therefore the reactive power is regulated to be zero. As a result, a proper control of Q_{gsc} can be accomplished with a single PI control loop, as shown in Fig. 7, where the current reference i_{qg}^* is set to zero.
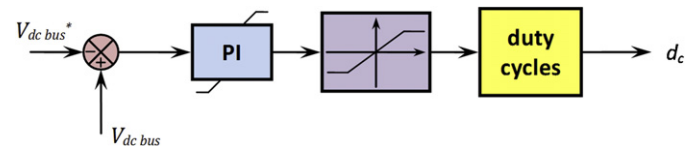

Fig. 8. Battery power converter control scheme.

5.4. Battery power converter control

This converter is controlled in order to maintain the DC bus voltage close to its nominal value (1150 V). As shown in Fig. 8, the voltage reference is compared with the actual measurement. The error between these signals is used in a PI controller in order to define the duty cycle that runs the IGBT switches of the power converter.

6. Supervisory control system

The hybrid system requires a supervisory control system that coordinates the performance of the both energy sources (wind turbine and ESS) and allows a reliable and controlled response. In this work, a state machine-based control system was developed in order to achieve the coordinate operation of the wind turbine and ESS.

This supervisory control sets the power reference to be stored in the battery, considering its SOC and the power mismatching between the power generated by the DFIG (P_g) and the power demanded by the grid (P_{demand}). Moreover, it activates the power reduction mode when the battery reaches its maximum SOC, and forces the battery charging when the SOC achieves the minimum level. Nevertheless, the battery will be controlled to supply the demanded power whenever the SOC is within the secure operation range (from 30 to 70% of the total capacity).

Seven different states depending on the battery SOC are considered. Changes between the SOC levels are performed according to Fig. 9, where two hysteresis cycles for the control of the level changes are shown. It avoids constant switching between bordering states.

The state machine was implemented using a truth table block available in Simulink. The input variables to the truth table are: the active power mismatching (calculated as the difference between the total power generated by the DFIG, P_g, and the power demanded by the grid), named *power unbalance*; the SOC of the battery; and the power flowing through the rotor windings, P_r. Two variables,
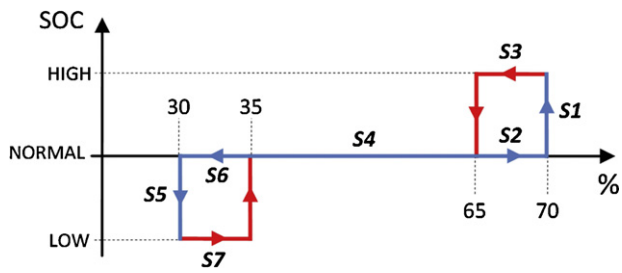
Fig. 9. Hysteresis cycles for the levels battery SOC.

Low_SOC and *High_SOC*, are internally used in the truth table. Finally, the output variables are the battery power reference (P_{batt}), and the switching signal *power reduction*, which indicates when this operating mode must be applied.

In the implemented truth table, each state is defined by a condition. When a certain condition is true, it calls an action, and then the corresponding instruction is generated. A summary of the control strategy applied to the supervisory control system is given in Table 1, where *NM* stands for *not modified* when the variable value does not change.

- *State 1*: SOC ≥ 70% → Action 1. This state is achieved when the battery reaches its maximum recommended SOC. As a consequence, the internal variable *High_SOC* is forced to 1, and the switching signal *power reduction* is also activated. Therefore, the active power reference will not be set as a function of the angular velocity, but as a predetermined value given by the power demand. Hence, the active power surpluses are avoided, and the battery stops charging. In addition, the battery power reference will be set to the minimum value between zero and *power unbalance*, thus allowing the discharge when *power unbalance* is negative.
- *State 2*: SOC ≥ 65% and High_SOC = 0 → Action 2. In this state, the battery has not reached its maximum SOC. Therefore, the RSC control will be operating with the optimization/limitation strategy, since *power reduction* is not active. In addition, either charging or discharging of the battery is allowed, so that the battery power reference will be set to compensate the power mismatching between generation and demand by using the *power unbalance*. As seen in Table 1, none of the internal variables are modified in this state.
- *State 3*: SOC ≥ 65% and High_SOC = 1 → Action 3. In this state, only the battery discharging is allowed. The *power reduction* mode is active, and the battery power reference is set to the minimum value between zero and *power unbalance*.
- *State 4*: 35% ≤ SOC ≤ 65% → Action 4. In this state, it is considered that the battery operates with normal SOC, and no restrictions are applied. Both internal variables *High_SOC* and *Low_SOC* are set to 0. The DFIG operates in the optimization/limitation mode, and the *power unbalance* is compensated with the battery power.
- *State 5*: SOC ≤ 30% → Action 5. At 30% the battery SOC reaches its low level. Below this value, severe damage can happen inside the device. Therefore, deeper discharge must be strictly avoided.

Table 1
Summary of the supervisory control system.

State/action	High_SOC	Low_SOC	Power reduction	P_{batt}
A1	1	NM	1	Min (0, power unbalance)
A2	NM	NM	0	Power unbalance
A3	NM	NM	1	Min (0, power unbalance)
A4	0	0	0	Power unbalance
A5	NM	1	0	Max (P_r, power unbalance)
A6	NM	NM	0	Power unbalance
A7	NM	NM	0	Max (P_r, power unbalance)

In this state, the variable *Low_SOC* is set to 1, and the battery recharging is forced by setting its power reference to the maximum value between the *power unbalance* and the absolute value of the power flowing through the RSC. Obviously, the *power reduction* mode will not be active in this state, since the maximum power generated by the DFIG is desirable.
- *State 6*: SOC ≤ 35% and Low_SOC = 0 → Action 6. In this state, the lowest SOC level has not been accomplished yet. Therefore, no restrictions of charge or discharge are applied to the battery. Since either positive or negative power references are permitted to the battery, the *power unbalance* will be the battery power reference.
- *State 7*: SOC ≤ 35% and Low_SOC = 1 → Action 7. Once the battery is discharged to its lowest value, the recharging process must take place at least until the SOC exceeds 35%. As a consequence, the battery power reference defined in state 5 is also valid in state 7. It avoids damaging the storage device due to excessively deep discharge cycles and guarantees an adequate recovery of the battery capacity.

7. Simulation results and discussion

The hybrid generation system (DFIG wind turbine with battery) and its control system were modeled and simulated in SimPowerSystems of MATLAB-Simulink. To evaluate the hybrid system, two different simulations were carried out, where the most relevant parameters were analyzed, such as active and reactive powers, rotating speed, blade pitch angle, DC bus voltage and battery SOC. In both cases, a variable wind time series was used as input variable to the wind turbine model, and the active power demanded by the grid was a user-defined variable. The first simulation focused on the hybrid system operation when the battery achieved low SOC. In this case, the battery recharging was required in order to avoid internal damage in the storage device. In the second simulation, the hybrid system operation with high battery SOC was illustrated, where the wind power generation was reduced in order to avoid generation surpluses, when the maximum SOC was reached.

7.1. Case 1: simulation with low battery SOC

In this simulation case, it was considered an initial battery SOC of 35%. With this SOC, the battery could provide or store energy.

The wind speed profile used in the first simulation is shown in Fig. 10. As seen, the incoming wind speed was kept below rated values (rated wind speed 12.5 m s^{-1}) during the first 95 s, while the wind turbine experienced winds above rated for the rest of the simulation.

The active power response, measured at different points of the hybrid system and expressed in pu units, is shown in Fig. 11. During the first 110 s, the active power demanded by the grid was 0.96 pu, which exceeded the available wind power. For this reason, the battery supplemented the output of DFIG in order to provide the demanded power, until it reached its lowest recommended SOC of 30% at 81.5 s (see Fig. 12). In that moment, a battery recharging cycle began and lasted until the SOC achieved 35% or higher. During the recharging time, the battery was charged by the power provided by the rotor windings and no active power was provided through the GSC. Therefore, the total output power of hybrid system was only the stator active power and the grid consumption could not be completely fulfilled. At 117 s, the power demanded by the grid was reduced below the stator output power until 0.4 pu. This power surplus was also stored in the battery, enabling a faster SOC increase. As observed in Fig. 12, the battery was discharged during the first 81.5 s, and charged during the rest of the simulation.

On the other hand, the reactive power reference was set to zero during the simulation, and therefore, it was considered that the
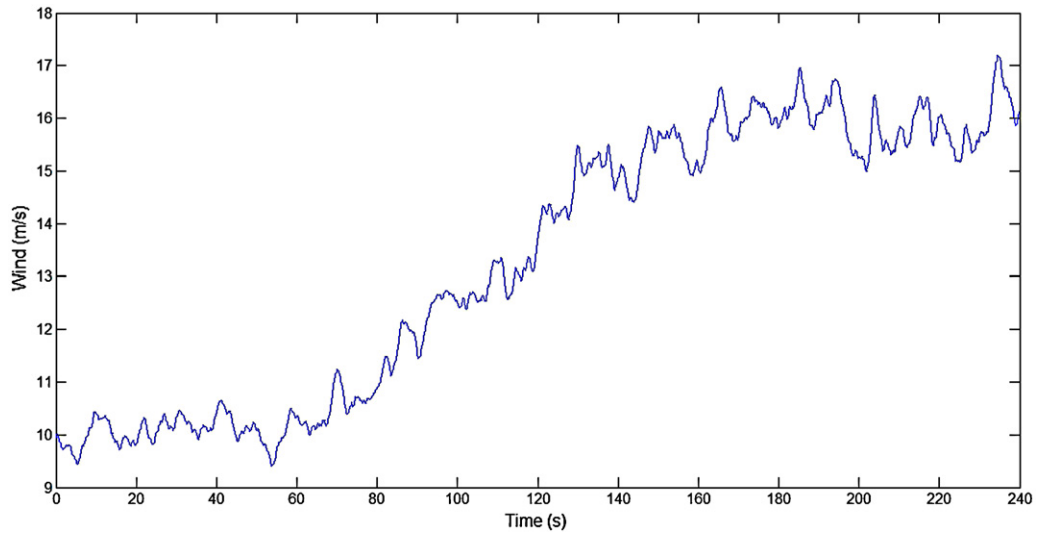
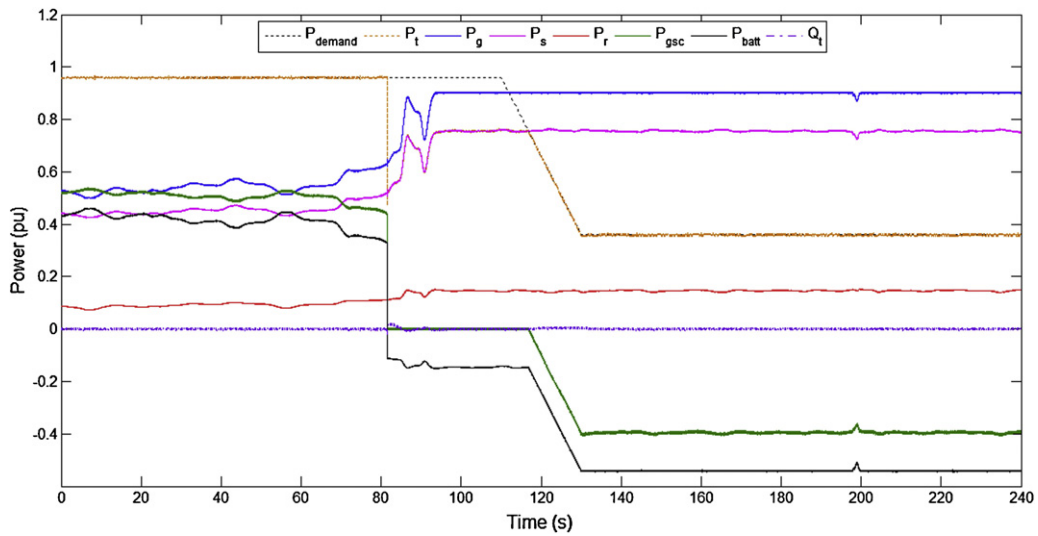**Fig. 10.** Wind speed profile for the simulation case 1.

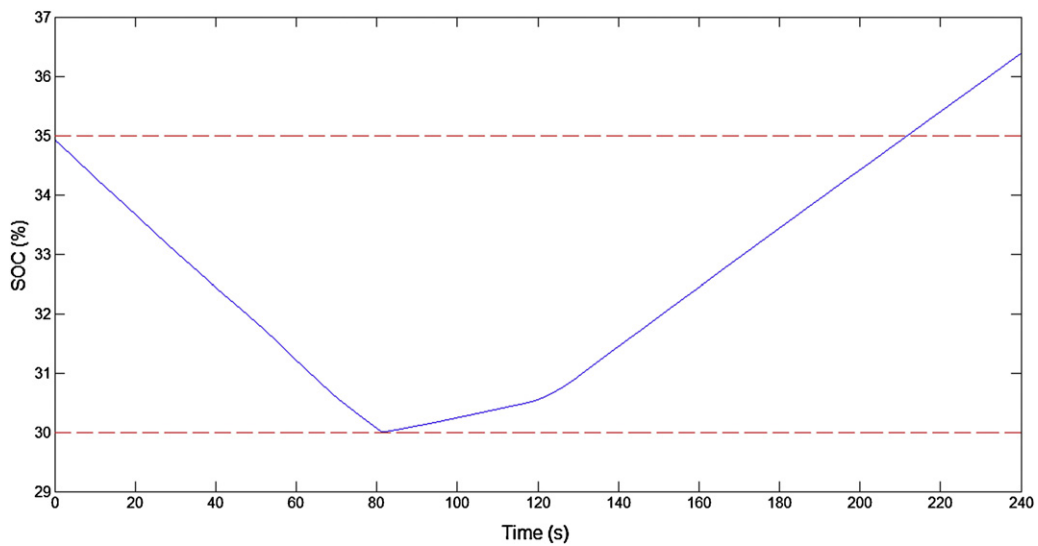**Fig. 11.** Active and reactive powers for the simulation case 1.

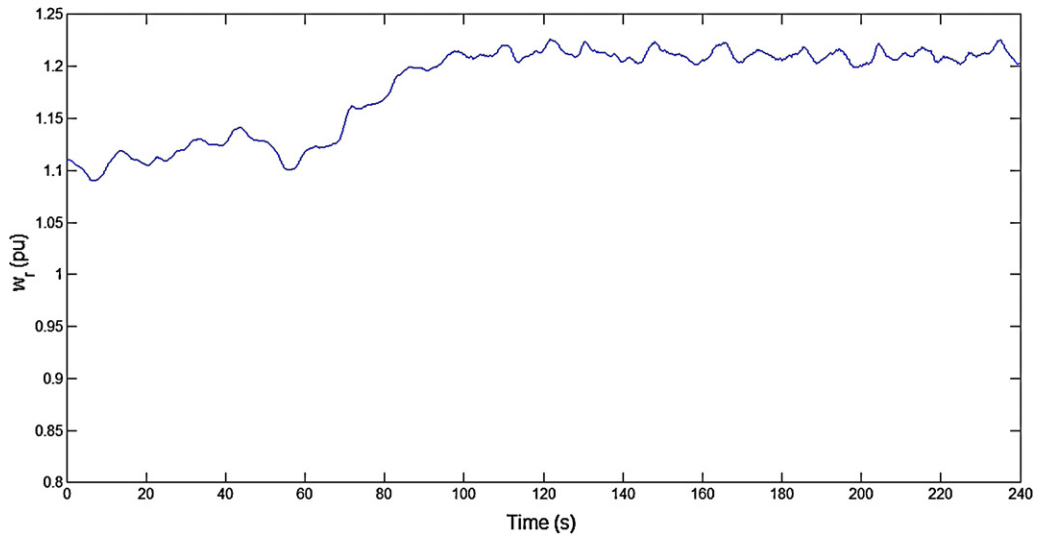
Fig. 12. Battery SOC for the simulation case 1.
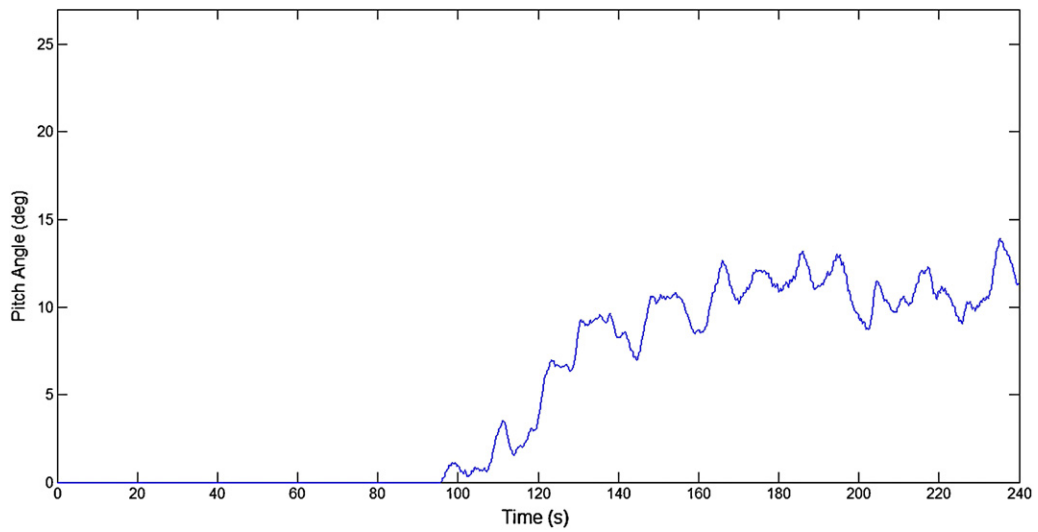
Fig. 13. Rotor speed.
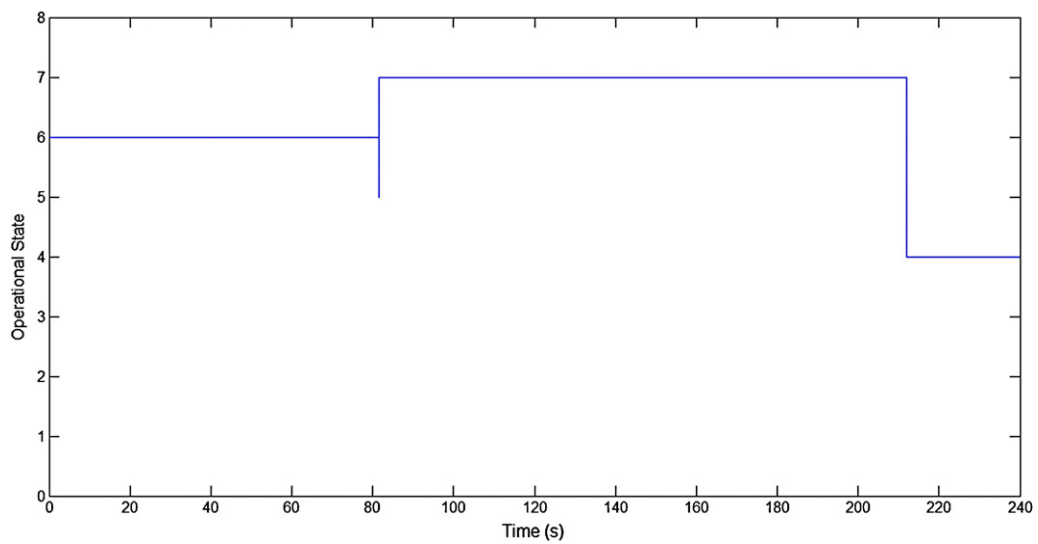

Fig. 14. Blade pitch angle.

Fig. 15. Operational states of the supervisory control system for the simulation case 1.
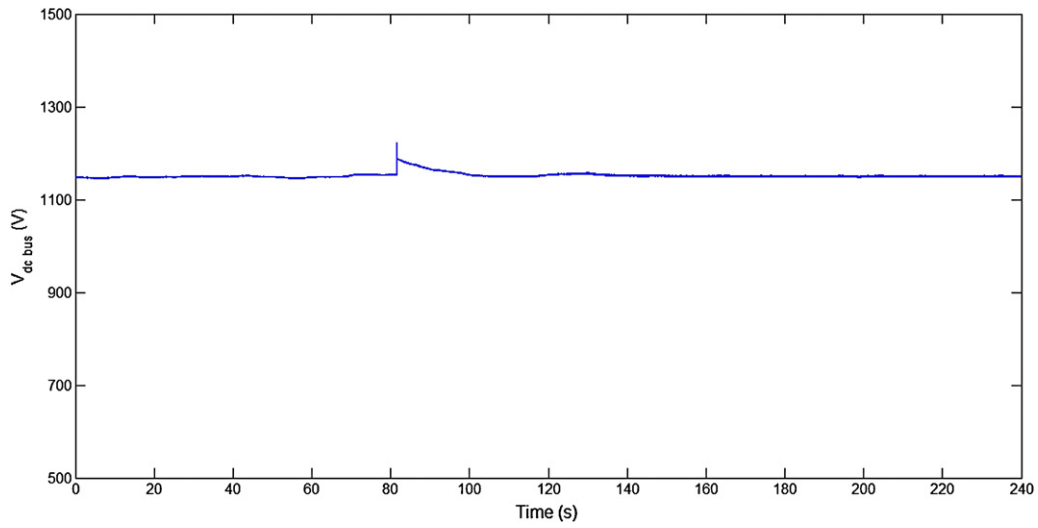
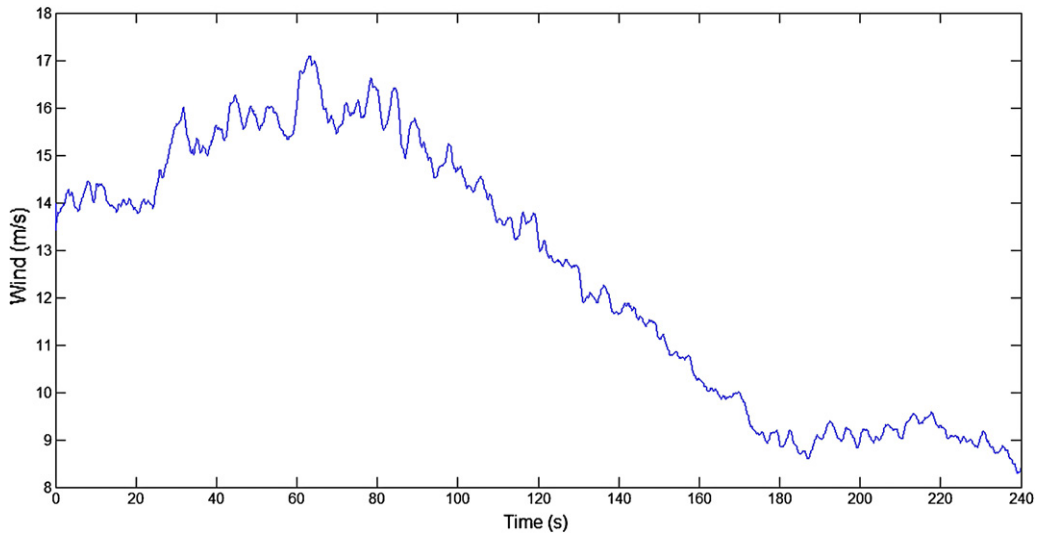**Fig. 16.** DC bus voltage.

Fig. 17. Wind speed profile for the simulation case 2.
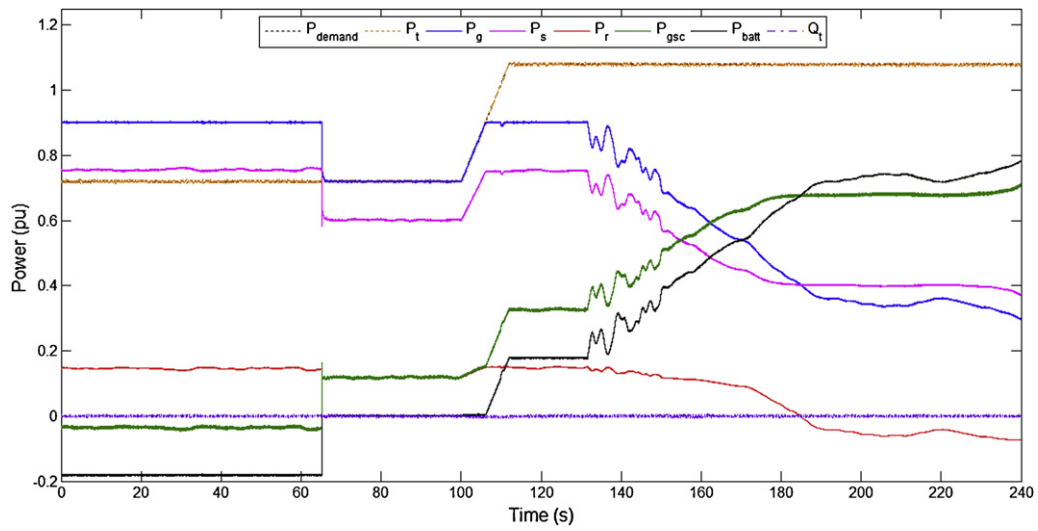

Fig. 18. Active and reactive powers for the simulation case 2.

system operated with unity power factor. Fig. 11 shows the reactive power Q_t measured at the grid connection point. As seen, a proper regulation of the reactive power was achieved.

For winds below rated (during the first 95 s), the rotor angular speed (Fig. 13) varied accordingly to the wind speed changes, since the blade pitch angle (Fig. 14) was set to the minimum value in order to maximize the power extracted from the wind. For winds above rated, the rotor angular speed varied close to the rated speed (1.2 pu), since the blade pitch controller acted on the pitch angle in order to limit the power extracted from the wind, and subsequently, the rotor speed.

Fig. 15 shows the operational states achieved by the supervisory control system during the simulation. The system began to work in state 6. In this state, no restrictions of charge or discharge were applied to the battery, and therefore, it could provide or store energy. At 81.5 s, the battery reached its lowest recommended SOC of 30%. Then, the system adopted temporary the state 5, since the battery recharging began immediately, the SOC started to increase until the system reached the state 7. During this operational state, the battery recharging took place until the SOC exceeded 35% at 212 s. Then, the system adopted the state 4, which was kept until the end of the simulation.

As mentioned previously, the battery was interconnected to the DC bus through a DC/DC converter, which was controlled in order to maintain the DC bus voltage at rated value. As shown in Fig. 16, it was achieved an appropriate control of the DC bus voltage.

7.2. Case 2: simulation with high battery SOC

In the second simulation, it was considered an initial battery SOC of 69%, which corresponded to the operational state 2. In this state, the battery could provide or store energy.

Fig. 17 shows the wind speed profile used in this simulation. As seen, the wind speed was kept above rated during the first 130 s. Then, the wind speed dropped, reaching a minimum average value of 9 m s^{-1} from 180 s to 240 s.

In this case, the active power demanded by the grid was set to 0.72 pu during the first 100 s. Then, the power demand increased up to 1.08 pu with a rising slope of 0.03 pu s^{-1}, as shown in Fig. 18. At the beginning of simulation, the DFIG generated its rated active power, but as the power demanded by the grid was less than rated the power excess was stored in the battery. However, the battery SOC reached 70% at 61 s (Fig. 19), and therefore the battery charging had to be stopped. Then, the *power reduction* mode was
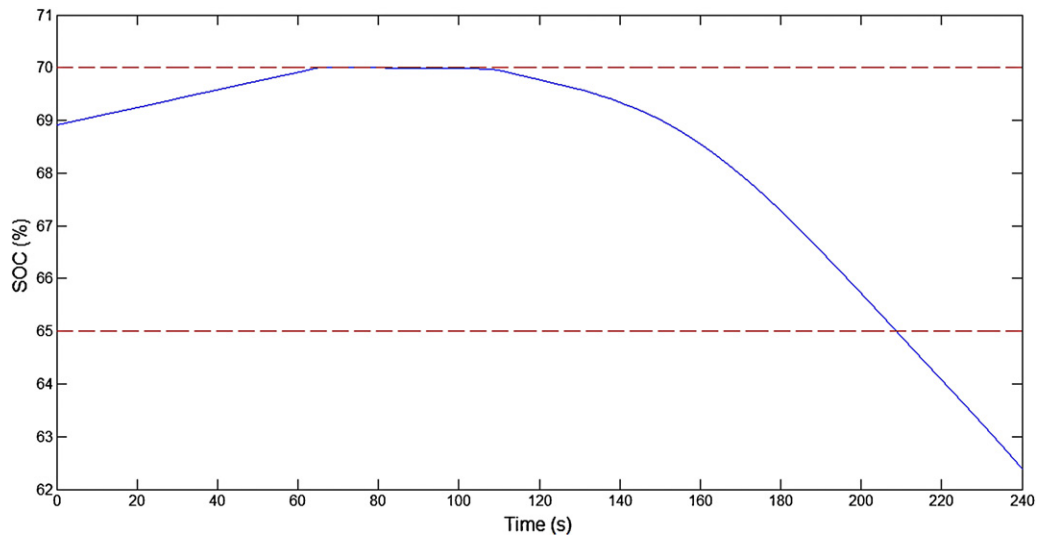

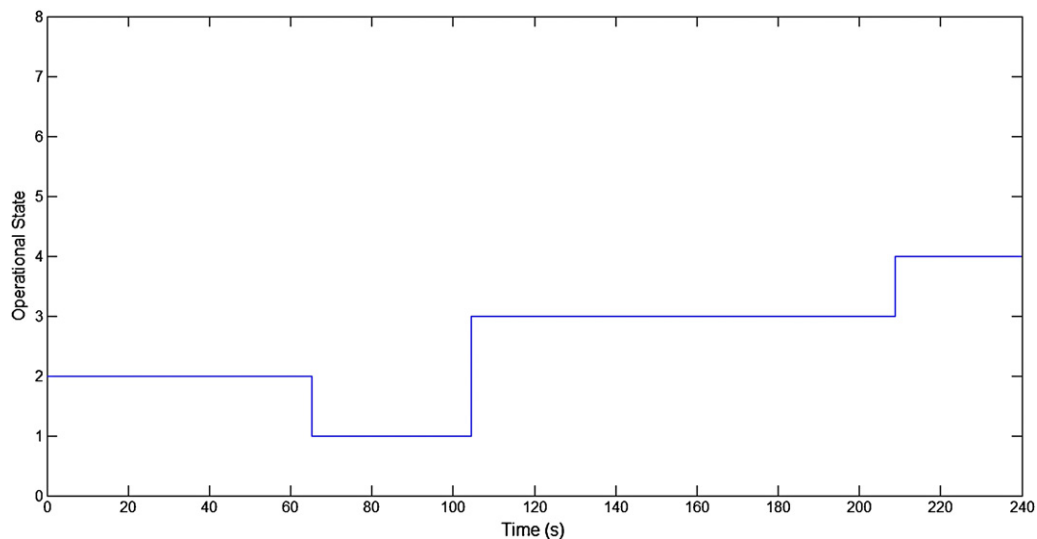**Fig. 19.** Battery SOC for the simulation case 2.

Fig. 20. Control states of the supervisory control system for the simulation case 2.

activated, and the total power generated by the DFIG was reduced and adjusted to the power demanded by the grid. The battery power reference was set to zero, avoiding either charge or discharge, and therefore, the power delivered with the grid through the GSC was equal to the RSC power. The battery SOC was kept at 70% until the hybrid system was demanded to generate more than the rated power of the DFIG, which occurred at 106 s. From that moment on, the extra power was provided by the battery, which led to its discharging for the rest of the simulation, as seen in Fig. 19. Once the SOC fell below 65%, the supervisory control system deactivated the *power reduction* mode.

As shown in Fig. 20, the battery SOC was above 65% at the beginning of the simulation, which corresponded to the operational state 2. As mentioned previously, the battery SOC reached 70% at 61 s, and then, the hybrid system adopted the operational state 1. While the battery SOC was kept at 70%, the supervisory control system remained in state 1. At 106 s, the hybrid system adopted the state 3, and the battery discharging started. Finally, the system changed to state 4, when the SOC decreased below 65%, at 208.8 s.

8. Conclusions

This paper has presented a model and control system to evaluate the coordinate operation of a grid connected hybrid power system, composed of 1.5 MW DFIG wind turbine and lead-acid battery as ESS.

In a DFIG wind turbine, vector control is applied to the power converters in order to regulate the active and reactive power exchanges with the grid. As a result, the wind turbine can adjust the active power output to the grid demands unless the maximum power demanded by the grid is the wind turbine rated power, and operate with unity power factor o with a certain reactive power regulation. However, the intermittency and variability of wind energy leads to uncontrolled fluctuations of the wind turbine output power. These power fluctuations can be reduced by connecting, through a bidirectional DC/DC converter, a battery to the DC bus of the DFIG. In this work, a supervisory control system based on a state machine control strategy is responsible for setting the battery power reference depending on the battery SOC and the operating conditions. Furthermore, the battery DC/DC converter is controlled to maintain the DC bus voltage at its rated value.

Simulations performed show that the hybrid system adapts appropriately to the changes in both wind speed and grid demand. The ESS provides or stores the power mismatching between the actual wind power and grid demand, whenever the battery SOC remains within the recommended limits. As a result, the hybrid system is able to provide constant power to the grid as the incoming wind varies, and increase the power transferred to grid, when required. On the other hand, the possibility to store energy surpluses allows maximum wind energy capture even when the power demand is low. This enables the possibility to decouple generation from demand, and optimize the energy. Other parameters that must be taken into account, such as reactive power and voltage, can be regulated by applying an adequate control strategy. Hence, the inclusion of an ESS does not negatively affect the proper operation of the wind turbine; on the contrary, it enhances the wind turbine capabilities, allowing a higher and less fluctuating power output to the grid.

References

[1] A. Pullen, L. Qiao, S. Sawyer (Eds.), Global Wind 2009 Report, Global Wind Energy Council, Brussels, 2010 http://www.gwec.net/index.php?id=167.
[2] M. Beaudin, H. Zareipour, A. Schellenberglabe, W. Rosehart, Energy Sustain. Dev. 14 (2010) 302–314.
[3] J. McDowall, J. Power Sources 162 (2006) 959–964.
[4] S. Teleke, M.E. Baran, A.Q. Huang, S. Bhattacharya, L. Anderson, IEEE Trans. Energy Convers. 24 (2009) 725–732.
[5] M. Black, G. Strbac, J. Power Sources 162 (2006) 949–953.
[6] V. Akhmatov, H. Knudsen, Electr. Power Syst. Res. 77 (2007) 1228–1238.
[7] P.J. Luickx, E.D. Delarue, W.D. D'haeseleer, Appl. Energy 85 (2008) 787–799.
[8] J.M. Carrasco, L.G. Franquelo, J.T. Bialasiewicz, E. Galvan, R.C.P. Guisado, A.M. Prats, J.I. Leon, N. Moreno-Alfonso, IEEE Trans. Ind. Electron. 53 (2006) 1002–1016.
[9] J.P. Barton, D.G. Infield, IEEE Trans. Energy Convers. 19 (2004) 441–448.
[10] S. Vazquez, S.M. Lukic, E. Galvan, L.G. Franquelo, J.M. Carrasco, IEEE Trans. Ind. Electron. 57 (2010) 3881–3895.
[11] S.A. Lone, M.U.D. Mufti, J. Power Sources 163 (2006) 604–615.
[12] H. Ibrahim, A. Ilinca, J. Perron, Renew. Sustain. Energy Rev. 12 (2008) 1221–1250.
[13] M. Perrin, P. Malbranche, E. Lemaire-Potteau, B. Willer, M.L. Soria, A. Jossen, et al., J. Power Sources 154 (2006) 545–549.
[14] I. Hadjipaschalis, A. Poullikkas, V. Efthimiou, Renew. Sustain. Energy Rev. 13 (2009) 1513–1522.
[15] K.C. Divya, J. Østergaard, Electr. Power Syst. Res. 79 (2009) 511–520.
[16] C.D. Parker, J. Power Sources 100 (2001) 18–28.
[17] Y. Chang, X.X. Mao, Y.F. Zhao, S.L. Feng, H.Y. Chen, D. Finlow, J. Power Sources 191 (2009) 176–183.
[18] X.F. Song, C.L. Xia, T.N. Shi, Appl. Energy 87 (2010) 3283–3293.
[19] L.M. Fernandez, C.A. Garcia, F. Jurado, Energy 33 (2008) 1438–1452.
[20] L.M. Fernandez, C.A. Garcia, F. Jurado, Renew. Energy 35 (2010) 1308–1318.
[21] S.M. Muyeen, R. Takahashi, T. Murata, J. Tamura, IEEE Trans. Energy Convers. 24 (2009) 740–749.
[22] M.J. Khan, M.T. Iqbal, Appl. Energy 86 (2009) 2429–2442.
[23] R.J. Mantz, H. De Battista, Int. J. Hydrogen Energy 33 (2008) 4291–4300.
[24] C. Abbey, G. Joos, IEEE Trans. Ind. Appl. 43 (2007) 769–776.
[25] General Electric Company, 1.5 MW series wind turbine. <http://www.gepower.com/prod_serv/products/wind_turbines/en/15mw/specs.htm>.
[26] SimPowerSystems™ Reference, Hydro-Québec/the MathWorks, Inc., Natick, MA, 2010.
[27] S. Heier, Grid Integration of Wind Energy Conversion Systems, John Wiley & Sons, Chichester, 1998.
[28] P. Krause, O. Wasynczuk, S.D. Sudhoff, Analysis of Electric Machinery, IEEE Press, 2002.
[29] Discover Energy Corp Datasheet Discover® D Series VRLA Industrial Batteries, part no. D21000. <http://www.discover-energy.com/files/datasheets/D21000.pdf>.
[30] P. Garcia, L.M. Fernandez, C.A. Garcia, F. Jurado, IEEE Trans. Ind. Electron. 57 (2010) 4013–4023.
[31] L.M. Fernandez, P. Garcia, C.A. Garcia, J.P. Torreglosa, F. Jurado, Int. J. Hydrogen Energy 35 (2010) 5731–5744.

Glossary

Abbreviations

CAES: compressed air energy storage
DFIG: doubly-fed induction generator
ESS: energy storage system
GSC: grid side converter
IGBT: insulated gate bipolar transistor
PMSG: permanent magnet synchronous generator
RSC: rotor side converter
SMES: superconducting magnetic energy storage
SOC: state-of-charge
VRLA: valve regulated lead-acid

Wind turbine parameters

A: area embraced by the rotor blades
C_p: wind turbine power coefficient
P_{wt}: wind turbine mechanical power
T_{wt}: wind turbine mechanical torque
u: wind speed
λ: tip speed ratio
θ: pitch angle
ρ: air density
ω_{wt}: wind turbine angular speed

Drive train parameters

D_{dt}, K_{dt}: damping factor and stiffness
F: viscous friction coefficient
J_r, J_{wt}: generator rotor and wind turbine inertia masses
T_e: generator electromechanical torque
T_{mec}: drive train mechanical torque

ω_r: generator rotor angular speed

Generator parameters

i_{dqg}, i_{abcg}: GSC current
i_{dqr}, i_{abcr}: rotor windings current
i_{dqs}, i_{abcs}: stator windings current
L_m: magnetizing inductance
L_r: rotor inductance
L_{RL}: filter inductance
L_s: stator inductance
p: number of pair poles
P_{demand}: active power demanded by the grid
P_g: DFIG total active power generation
P_{gsc}: active power flow through the GSC
P_r: active power generation through the rotor windings
P_s: active power generation through the stator windings
P_t: total active power delivered to grid
Q_{gsc}: reactive power flow through the GSC
Q_s: reactive power flow through the stator windings
Q_t: total reactive power delivered to grid
R_r: rotor resistance
R_{RL}: filter resistance

R_s: stator resistance
u_{dqg}, u_{abcg}: GSC voltage
u_{dqr}, u_{abcr}: rotor voltage
u_{dqs}, u_{abcs}: stator voltage
$V_{dc\ bus}$: Dc bus voltage
φ_{dqr}: rotor windings magnetic flux
φ_{dqs}: stator windings magnetic flux
ω: synchronous speed

Battery parameters

E_0: constant voltage
E_{bat}: no load voltage
f_{hyst_char}: battery hysteresis during charge
f_{hyst_disch}: battery hysteresis during discharge
i^*: low-frequency current dynamics
i: battery current
i_t: extracted capacity
K: polarization constant
P_{batt}: battery active power reference
Q: maximum capacity
R_i: internal resistance
U_{bat}: battery output voltage